An In-Depth Evaluation of Heritage Algorithms for Snow Cover and Snow Depth Using AMSR-E and AMSR2 Measurements

YONG-KEUN LEE

Cooperative Institute for Meteorological Satellite Studies, University of Wisconsin–Madison, Madison, Wisconsin

CEZAR KONGOLI

Cooperative Institute for Climate and Satellites, University of Maryland, College Park, College Park, Maryland

JEFFREY KEY

Center for Satellite Applications and Research, NOAA/NESDIS, Madison, Wisconsin

(Manuscript received 5 May 2015, in final form 24 September 2015)

ABSTRACT

The Advanced Microwave Scanning Radiometer 2 (AMSR2) was launched in 2012 on board the *Global Change Observation Mission 1st–Water* (*GCOM-W1*) satellite. This study presents a robust evaluation of AMSR2 algorithms for the retrieval of snow-covered area (SCA) and snow depth (SD) that will be used operationally by the National Oceanic and Atmospheric Administration (NOAA). Quantitative assessment of the algorithms was performed for a 10-yr period with AMSR-E and a 2-yr period with AMSR2 data using the NOAA Interactive Multisensor Snow and Ice Mapping System (IMS) snow cover and in situ SD data as references. AMSR-E SCA showed a monthly overall accuracy rate of about 80% except in May. Accuracy improves significantly to over 90% when wet snow cases are excluded, and accuracy differences between ascending and descending portions of orbits also decrease. Microwave-derived SCA over dry snow areas can therefore be obtained with accuracy close to optically derived SCA. An evaluation of the results for AMSR-E SD showed a low overall bias of 1 cm and a root-mean-square error of 20 cm. Results for AMSR2-based SCA and SD are similar to those from AMSR-E. Biases and root-mean-square errors show dependencies on elevation, forest fraction, the magnitude of snow depth, and snow cover class.

1. Introduction

Snow is one of the most dynamic hydrological variables on the earth's surface and is the cryospheric component with the largest seasonal variation in spatial extent. Over Northern Hemisphere lands, snow cover ranges from about $45.2 \times 10^6\,km^2$ in January to $1.9 \times 10^6\,km^2$ in August (Barry et al. 2007). Because of its dramatic seasonal variation and high reflectivity, snow plays a key role in the global energy and water budget (Barry et al. 2007; IPCC 2007). Snow affects regional and global climate by modulating the atmosphere (Barry 2002; Barry et al. 2007; Cohen 1994; Cohen and Entekhabi 1999; Walsh 1984). For example, Cohen and Entekhabi (1999) showed that early-season Eurasian snow cover and the Siberian high pressure system affect Northern Hemisphere winter atmospheric circulation and suggested that information on the snow cover distribution can be very useful in winter climate prediction. The hydrologic importance of snowmelt also has been actively discussed (Dyer 2008; Hamlet and Lettenmaier 1999; Yang et al. 2003; Zhang et al. 2001).

Satellite remote sensing is the primary tool for mapping the global distribution of snow parameters such as the snow-covered area (SCA), snow depth (SD), and snow water equivalent (SWE). Both optical and microwave satellite measurements have been used to retrieve SCA. However, SWE and SD are nearly impossible to measure directly from optical imagery because the electromagnetic radiation emanating from the top few centimeters of snow dominates the remote sensing signal at optical wavelengths. In addition, snow retrievals

Corresponding author address: Yong-Keun Lee, CIMSS, University of Wisconsin, 1225 W. Dayton St., Madison, WI 53706.
E-mail: yklee@ssec.wisc.edu

DOI: 10.1175/JTECH-D-15-0100.1

TABLE 1. AMSR-E/AMSR2 snow property retrieval algorithms used in this study.

	Algorithms or methods
Snow cover	- Grody's SCA algorithm (Grody 1991; Grody and Basist 1996) - enhancements : Snow climatology (NESDIS weekly snow frequency 1973–2000) : Wet snow filter (Tedesco and Narvekar 2010)
Snow depth	- Kelly's SD algorithm (Kelly 2009) over AMSR-E/AMSR2-detected snow cover

from optical satellite measurements require clear-sky conditions and sufficient daylight. Microwave radiation is unhindered by darkness and clouds and penetrates a deeper layer of snow cover.

Passive microwave measurements collected from different satellite sensors—for example, the Scanning Multichannel Microwave Radiometer (SMMR)(Chang et al. 1987), the Special Sensor Microwave Imager (SSM/I) (Grody 1991; Grody and Basist 1996), the Special Sensor Microwave Imager/Sounder (SSMIS) (Sun and Weng 2008), the Advanced Microwave Sounding Unit (AMSU) (Ferraro et al. 2005), and the Advanced Microwave Scanning Radiometer for the Earth Observing System (AMSR-E) (Kelly 2009; Tedesco and Narvekar 2010)—have been used for global retrievals of SCA, SD, and SWE. The Advanced Microwave Scanning Radiometer 2 (AMSR2) instrument is a passive microwave instrument launched in 2012 on board the *Global Change Observation Mission 1st–Water* or "*Shizuku*" (*GCOM-W1*) satellite (http://suzaku.eorc.jaxa.jp/GCOM_W/w_amsr2/whats_amsr2.html). It is effectively a replacement for AMSR-E (launched in May 2002 on board *Aqua*), which stopped regular scanning in October 2011.

The main objective of this study is to conduct an in-depth assessment of heritage SCA and SD algorithms applied to AMSR2 data that have been implemented for operational use at the National Oceanic and Atmospheric Administration (NOAA) (see Table 1). The SCA algorithm is based on the decision tree classification method of Grody (1991) and Grody and Basist (1996, referred to as Grody's SCA algorithm) with snow climatology tests and wet snow filter as enhancements that are introduced here. The SD algorithm is based on the current NASA AMSR-E SD algorithm described fully in Kelly (2009, referred to as Kelly's SD algorithm). This is an enhanced version of the original NASA AMSR-E SD baseline algorithm (Chang et al. 1987) that computes SD dynamically using adjustable coefficients to account for spatially and temporally varying snow grain size. While Grody's SCA algorithm was developed for SSM/I, applications to SSMIS and AMSU data have been documented and evaluated (Ferraro et al. 2005; Grody et al. 2000; Grody and Basist 1996; Kongoli et al. 2007; Sun and Weng 2008). This is the first assessment of the algorithm and its new enhancements using AMSR-E/AMSR2 measurements.

This study significantly extends the validation efforts of Kelly (2009), who used 2 years of in situ SD data, and Tedesco and Narvekar (2010), who used 3 years of SD data from the National Operational Hydrologic Remote Sensing Center (NOHRSC) Snow Data Assimilation System (NOHRSC 2004) and the World Meteorological Organization (WMO) (http://www.ncdc.noaa.gov). Here we use 10 years of AMSR-E and 2 years of AMSR2 data and a more comprehensive analysis of performance dependencies on elevation, forest fraction, snow depth, and snow class. This type of error analysis provides the uncertainty information needed for variational data assimilation and optimal interpolation techniques. For example, a blended analysis of SD has been developed operationally at NOAA and integrated into the Interactive Multisensor Snow and Ice Mapping System (IMS) (Kongoli and Helfrich 2015). The analysis blends in situ and microwave SD data using the optimal interpolation method (Brasnett 1999) and requires uncertainty SD information as input. Of additional value to these assimilation approaches is the quantification of uncertainties with respect to geomorphic attributes such as elevation and surface type, and seasonality, which are explored in depth here.

2. Data and methods

a. The AMSR-E and AMSR2 instruments

AMSR-E is a passive microwave radiometer sensing microwave radiation at six frequencies ranging from 6.9 to 89.0 GHz with fields of view from approximately 5 to 50 km (Table 2). This microwave radiometer on board the polar-orbiting satellite (*Aqua*) operationally provided snow properties (SCA and SWE; Tedesco and Narvekar 2010) until it failed in regular scanning as a result of an antenna problem in October 2011. AMSR2 is a microwave instrument that was launched in 2012 on board the *GCOM-W1* satellite. Now that *GCOM-W1* is part of the "A-Train" constellation along with *Aqua*, AMSR2 is considered as the successor to AMSR-E but with several enhancements: larger main reflector, additional 7.3-GHz channels, an improved calibration system (Imaoka et al. 2010), and improved spatial resolution (Table 2). Since AMSR-E and AMSR2 have the same center frequencies and corresponding band widths, AMSR-E brightness temperatures are used as

TABLE 2. Comparison of AMSR2, AMSR-E (Imaoka et al. 2010), and SSM/I sensor (Hollinger et al. 1990) features.

AMSR2	Center frequency (GHz)	6.9/7.3	10.7	18.7	23.8	36.5	89.0
	Bandwidth (MHz)	350	100	200	400	1000	3000
	IFOV (km × km)	35 × 62	24 × 42	14 × 22	15 × 26	7 × 12	3 × 5
AMSR-E	Center frequency (GHz)	6.9	10.7	18.7	23.8	36.5	89.0
	Bandwidth (MHz)	350	100	200	400	1000	3000
	IFOV (km × km)	43 × 75	29 × 51	16 × 27	18 × 32	8 × 14	4 × 6
SSM/I	Center frequency (GHz)			19.4	22.2	37.0	85.5
	Bandwidth (MHz)			240	240	900	1400
	IFOV (km × km)			69 × 43	60 × 40	37 × 29	15 × 13

proxies for AMSR2 in this study. Level 2A half-orbit AMSR-E brightness temperature products (V12) and level 1B half orbit of AMSR2 brightness temperature products (L1SGBTBR) are used in this study.

b. *Interactive Multisensor Snow and Ice Mapping System*

IMS is an interactive, operational snow and ice mapping system. It was originally introduced in 1999 based on the Ramsay (1998) method of producing daily maps over the Northern Hemisphere at 24-km resolution. In March 2004, the spatial resolution of the IMS snow products was further increased to 4 km (Helfrich et al. 2007).

To generate snow extent maps, analysts primarily rely on the visible imagery from polar-orbiting and geostationary satellites. The imagery from geostationary satellites is utilized in the form of animations, which help to distinguish moving clouds from snow. Quite often analysts visually observe and map the distribution of snow cover through semitransparent clouds. This is an obvious advantage compared to automated techniques based on visible wavelengths where most clouds prevent a reliable characterization of the land surface. Since 2006, the upgraded IMS has access to several automated snow and ice products generated at NOAA and NASA, as well as surface in situ SD reports. Recently analysts also began using images from live-streaming web cameras throughout the world (Kongoli et al. 2012). The availability of these additional sources of information has substantially enhanced the potential of analysts to accurately reproduce the snow cover distribution, especially in the case of persistent cloud cover, which precludes the use of visible imagery. IMS maps of snow and ice cover are considered the primary NOAA snow cover product and are incorporated into all global and mesoscale operational numerical weather prediction models run by NOAA's National Centers for Environmental Prediction (NCEP). IMS maps are updated daily, making them potentially useful for various environmental and practical applications at regional and local scales (http://www.natice.noaa.gov/ims). A more detailed discussion on NOAA's snow cover products including IMS is given in Kongoli et al. (2012). The IMS is currently being upgraded to generate snow and ice maps at 1-km resolution. Another important upgrade is the incorporation of a blended snow depth analysis into its 4-km product (S. Helfrich 2014, personal communication).

c. *In situ measured SD*

NOAA's National Environmental Satellite, Data, and Information Service (NESDIS) provides daily SD information from the Global Telecommunication System (GTS) in land surface synoptic observations (SYNOP) format, aviation routine weather report (METAR) format, and U.S. National Weather Service (NWS) Cooperative Observer (COOP) network format, which were used as ground truth to evaluate AMSR-E and AMSR2 SD. GTS and METAR SD were acquired via a data management and visualization system called the Man Computer Interactive Data Access System (McIDAS) (http://www.ssec.wisc.edu/mcidas/). The U.S. COOP SD data were acquired via NOAA's Climate Prediction Center (CPC). These datasets are also available at NOAA's National Climatic Data Center (NCDC) (https://www.ncdc.noaa.gov).

The locations of the ground sites (snow reported) available on 15 January 2008 are shown in Fig. 1. If there is no snow, WMO synoptic stations do not report SD (Brasnett 1999), and thus the number of WMO's reporting stations varies during the snow season. The COOP network is the oldest and largest U.S. ground observation network with currently more than 11 000 stations collecting data since 1981. Trained volunteers perform hydrometeorological measurements under the supervision of NOAA's NWS (http://www.weather.gov/rah/coop), which also acquires quality controls and distributes the data. Several thousand stations report a daily summary that includes minimum and maximum temperatures, snowfall, and SD.

d. *SCA retrieval algorithm*

Grody's SCA retrieval algorithm is based on a decision tree classification method that is described in detail in Grody (1991) and Grody and Basist (1996).

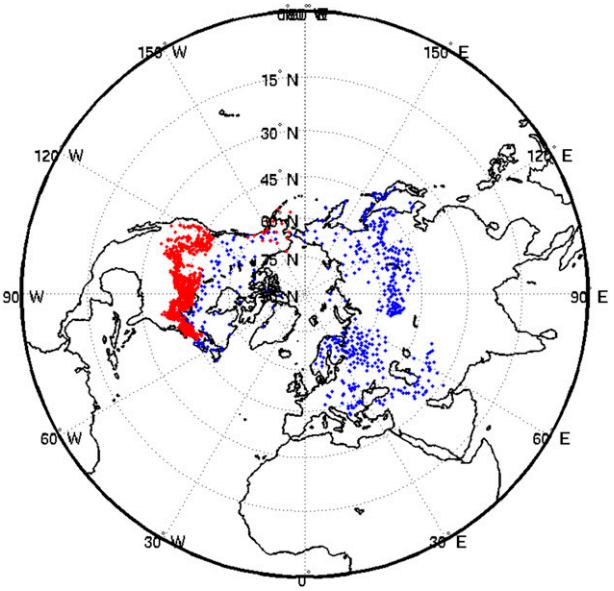

FIG. 1. The (snow reported) location of the surface synoptic observation stations (WMO GTS and surface METAR reports: 558, blue dots) and U.S. cooperative stations (1084, red dots) on 15 Jan 2008.

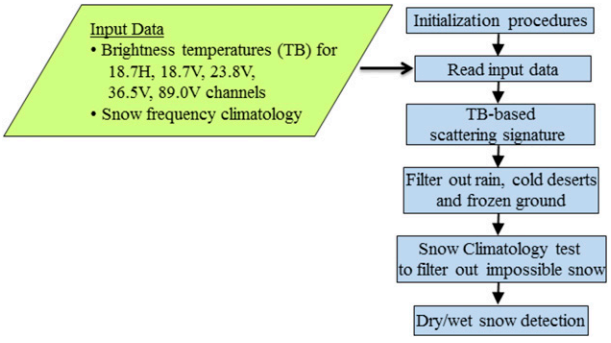

FIG. 2. AMSR2 high-level flowchart to detect SCA. The thresholds for brightness temperature–based scattering signature test and rain/cold deserts/frozen ground filtering are the same as those in Grody and Basist (1996).

Scattering surfaces (snow, deserts, rain, and frozen ground) and nonscattering surfaces (vegetation, bare soil, and water) are separated using brightness temperature–based scattering indices, followed by the application of additional brightness temperature–based thresholds to remove confounding factors (e.g., rain, frozen ground, and cold deserts). The algorithm was first applied to SMMR and SSM/I observations and later adopted for application to the AMSU instrument (Ferraro et al. 2005; Grody et al. 2000; Kongoli et al. 2007). Most recently Grody's SCA algorithm has been applied to SSMIS data (Sun and Weng 2008). To the authors' knowledge, this is the first time that Grody's SCA algorithm has been applied to AMSR-E or AMSR2 data.

Figure 2 presents a high-level flow diagram of Grody's SCA algorithm applied to AMSR-E/AMSR2 data over land. In this study, an AMSR-E/AMSR2 pixel is considered as land where the land mask is 100% at 6.9 GHz in order to minimize the water body effects. The land mask value is available as ''Land/Ocean_Flag_for6_10_18_23_36_50_89A'' for AMSR-E or ''Land_Ocean_Flag'' for AMSR2 in the same file as the half-orbit level 2A AMSR- E and level 1B AMSR2 brightness temperature products. The brightness temperature differences between 18.7 and 36.5 GHz and between 23.8 and 89 GHz (all vertically polarized) are used as scattering indices to separate scattering (difference is larger than 0) from nonscattering surfaces, followed by additional tests to remove warm and convective rain, cold deserts, and frozen ground from the scattering surfaces indicated by the two brightness temperature differences.

To further reduce errors of false snow identification, a snow climatology test has been added to Grody's SCA algorithm. This test compares the pixels identified as snow by Grody's SCA algorithm to a weekly snow frequency (probability) dataset at 1/3° latitude/longitude spatial resolution derived from processing NESDIS weekly snow maps available at the same resolution for the period 1973–2000 (http://www.cpc.ncep.noaa.gov/data/snow/). If the probability of snow is zero, then the snow identification of the pixel is rejected and the pixel is labeled as ''no snow.'' Next, a wet snow test adopted from the operational NASA AMSR-E SWE algorithm has also been added. A snow pixel is classified as ''dry'' when $TbH36 < 245$ K and $TbV36 < 255$ K, where TbV and TbH are vertically and horizontally polarized brightness temperatures, respectively (Tedesco and Narvekar 2010). This test is used in this study to detect wet snow and to compare SCA and SD performance statistics with and without wet snow cases. In Table 1, the SCA detection algorithm used in this study is shown.

e. SD retrieval algorithm

While the original NASA AMSR-E ''baseline'' operational algorithm assumes that SD and SWE are linearly dependent on the brightness temperature spectral difference at 18.7 and 36.5 GHz based on methods described in Chang et al. (1987) and Chang et al. (1997), the current NASA AMSR-E SWE algorithm is based on the Kelly (2009) method of SD retrieval and an ancillary snow density climatology data (Tedesco and Narvekar 2010). The main difference between the Kelly (2009) method and the original

baseline algorithm is the calculation of dynamical coefficients relating SD to brightness temperature spectral gradients, as well as the use of a channel available on the AMSR-E instrument that is not available on either SSM/I or SMMR, for example, the 10.7-GHz channel. Kelly's SD algorithm is based on the following empirical formulation:

$$\begin{aligned} \mathrm{SD(cm)} = \mathrm{ff}\left[p1\frac{(\mathrm{TbV18}-\mathrm{TbV36})}{(1-\mathrm{fd0.6})}\right] \\ + (1-\mathrm{ff})[p1(\mathrm{TbV10}-\mathrm{TbV36}) \\ + p2(\mathrm{TbV10}-\mathrm{TbV18})], \end{aligned} \tag{1}$$

where

$$\begin{aligned} p1 &= \frac{1}{\log10(\mathrm{TbV36}-\mathrm{TbH36})}, \\ p2 &= \frac{1}{\log10(\mathrm{TbV18}-\mathrm{TbH18})}. \end{aligned} \tag{2}$$

Forest fraction (ff) is from the MODIS Land Cover Type (MCD12Q1) International Geosphere–Biosphere Programme (IGBP) classification (LCSCG 2012). IGBP surface type has approximately $500 \times 500\,\mathrm{m}^2$ in gridcell resolution, and ff is calculated by considering the pixels around the center location of an AMSR-E pixel within a 7-km radius. Forest density (fd) is from the MODIS Vegetation Continuous Fields (VCF; MOD44B) product (Townshend et al. 2011). VCF has $250 \times 250\,\mathrm{m}^2$ in gridcell resolution and is circularly smoothed around the center location of an AMSR-E pixel within a 7-km radius.

In Eq. (1), SD of the forest snow composite is computed as the sum of SD over the forest and nonforest snow components. Forested SD is computed from the brightness temperature difference at 18.7 and 36.5 GHz in proportion to the vegetation fraction ff, whereas nonforest SD is computed from both the TbV10 − TbV18 and TbV10 − TbV36 in proportion to the snow fraction (1 − ff). Use of the TbV10 − TBV18 over snow is justified by its sensitivity to deep snow. Note that the coefficients in Eq. (1) are variable and computed from brightness temperature polarization differences [Eq. (2)]. The effect of complex topography has not been considered in this study since recent studies did not find obvious retrieval contamination from topographical factors (Dong et al. 2005; Vuyovich and Jacobs 2011; Vuyovich et al. 2014). For example, Vuyovich et al. (2014) suggested that errors from topography of the ground can be averaged out or the saturation in the microwave signal by deep snow can be more significant. In this study, SD is calculated only over pixels identified as snow using Grody's SCA algorithm. In Table 1, the SD calculation algorithm used in this study is shown.

f. Evaluation methodology

The SCA was generated from AMSR-E/AMSR2 data by applying Grody's SCA algorithm including the snow climatology and wet snow tests. The SD was also generated from AMSR-E/AMSR2 data by applying the Kelly (2009) algorithm.

An evaluation of SCA is performed using 24- and 4-km IMS products as "ground truth" references. The evaluation period includes five consecutive days (13–17) of each month between June 2002 and September 2011 for AMSR-E and five consecutive days (13–17) of each month between August 2012 and May 2014 for AMSR2. A sample of five consecutive days of each month was selected to reduce the computational burden. In this study, the term "monthly" indicates the results for these 5 days. For the collocation between IMS and AMSR-E/AMSR2 pixels, the closest IMS pixel is searched around an AMSR-E/AMSR2 pixel. Correct detection is counted when both AMSR-E/AMSR2 and IMS report snow (or no snow), while errors are counted when AMSR-E/AMSR2 reports snow (no snow) and IMS reports no snow (snow).

Four statistical parameters are computed to evaluate SCA: overall accuracy, snow detection rate, omission error (snow missing rate), and commission error (false alarm rate). These statistics are computed for the descending and ascending orbits, and with respect to forest fraction, elevation, and dry/wet snow. The overall accuracy is calculated as the number of pixels where both AMSR-E/AMSR2 and IMS detect snow or no-snow divided by the whole number. The whole number is the sum of the number of pixels that are reported as snow or no snow by both AMSR-E/AMSR2 and IMS. Omission error is calculated as the number of pixels where AMSR-E/AMSR2 misses snow divided by the whole number. Commission error is calculated as the number of pixels where AMSR-E/AMSR2 incorrectly detects snow divided by the whole number. In this study, the term, "false alarm" (commission error) is used to indicate a situation where IMS reports no snow and AMSR-E/AMSR2 reports snow. Snow detection rate is calculated as the number of pixels where both AMSR-E/AMSR2 and IMS detect snow divided by the number of pixels where IMS detects snow. The expressions for computing each parameter are shown in Table 3 giving each category, denoted as A, B, C, and D.

Evaluation of SD is performed against in situ measured SD for five consecutive days in winter months

TABLE 3. Confusion matrices for AMSR-E SCA product against IMS data. Overall accuracy = (A + D)/(A + B + C + D); omission error (snow missing rate) = C/(A + B + C + D); commission error (false alarm rate) = B/(A + B + C + D); and snow detection rate = A/(A + C).

	IMS snow	IMS no snow
AMSR-E snow	A	B
AMSR-E no snow	C	D

(January, February, and December) between December 2002 and February 2011 for AMSR-E and between December 2012 and February 2014 for AMSR2. Statistics include the root-mean-square (RMS) error and bias for the ascending and descending orbits, and with respect to forest fraction, elevation, and in situ SD. For the collocation between in situ SD locations and AMSR-E/AMSR2 pixels, the closest in situ SD within a 10-km radius of an AMSR-E/AMSR2 pixel is used. The 10-km radius from an AMSR-E/AMSR2 pixel is the approximate medium value of the instantaneous field of view (IFOV) size for the channels used in SD calculation.

3. Results and discussion

a. Assessment of SCA

Figure 3 presents monthly statistics of AMSR-E SCA with respect to 24-km IMS over the Northern Hemisphere. Results are shown with two bars (above and below) for each point in Figs. 3a and 3c, indicating ascending and descending orbits, respectively. Overall monthly accuracy is about 80% except in May. The decreased overall accuracy rate in May could be attributed to an increase in snowmelt coverage that resulted in a larger omission error (underestimation of snow coverage) and a lower snow detection rate. The omission error is larger than the commission error each month. This demonstrates that AMSR-E SCA tends to map less snow, which is consistent with Liang et al. (2008), who showed that the commission error of AMSR-E SCA compared with climate stations is less than the omission error. Since any snow signal can be dismissed if the snow covers only a small portion of the AMSR-E field of view (28 km × 16 km at 18.7 GHz), the underestimation of SCA using AMSR-E measurements may also be due to the coarse resolution of AMSR-E when compared to point station data (Liang et al. 2008).

The omission error shows a clear seasonal pattern, whereas the commission error shows little seasonal variation and stays below 5%. In Fig. 3a, the descending orbit shows a higher overall accuracy rate and snow detection rate than the ascending orbit. Also, the descending orbit shows a smaller omission error than the ascending orbit but a larger commission error. However, the commission error is less than 5% for both orbits except in October for the descending orbit (6%). Since descending orbits have an equator crossing time of 0130 local time (LT) (morning time series) and ascending orbits cross the equator at 1330 LT (afternoon time series), ascending orbits may have higher-frequency variability in microwave brightness temperature driven by atmospheric temperature effects than descending orbits (Foster et al. 1984; Markus et al. 2006) and daily thaw and freeze cycles.

Figures 3c and 3d show error statistics and the number of pixels for only AMSR-E-based dry snow cases. Wet snow cases were excluded by applying the wet snow filters. The application of wet snow filters primarily reduces the large portion (92%) of no-snow pixels from AMSR-E measurements, implying that wet snow may be detected as bare land (Foster et al. 1984), while a small portion (5%) of AMSR-E snow pixels are excluded by the wet snow criteria as shown in Figs. 3b and 3d. The observation recorded during ascending orbit is affected more by the wet snow filters than that of the descending orbit. The pixels removed are not counted for accuracy and error calculations in Fig. 3c. When wet snow is excluded from the analysis, overall accuracy, snow detection rate, and omission error are significantly improved and the difference in accuracy between descending and ascending orbits is reduced. On the other hand, the commission error is not significantly impacted (Figs. 3a and 3c). The reduction of the difference in accuracy between the two orbits indicates that the capability of snow cover detection using descending and ascending orbit microwave measurements is similar for dry snow (Derksen et al. 2000).

Armstrong and Brodzik (2001) showed that passive microwave data underestimate snow extent in November and, to a lesser degree, in December compared to the NOAA weekly snow extent product (visible band remote sensing) as a result of the inability of passive microwave measurements to detect thin and intermittent snow cover. They also showed that the omission error decreases as winter progresses, because deeper snow enables more accurate detection of snow cover by passive microwave measurements. Regardless of the wet snow exclusion, the omission error shows a decreasing trend from October to December and as winter progresses (January and February) through March (Figs. 3a and 3c), which is consistent with Armstrong and Brodzik (2001). Interestingly, the descending orbit still shows a smaller omission error and larger commission error than the ascending orbit over dry snow. Tedesco and Wang

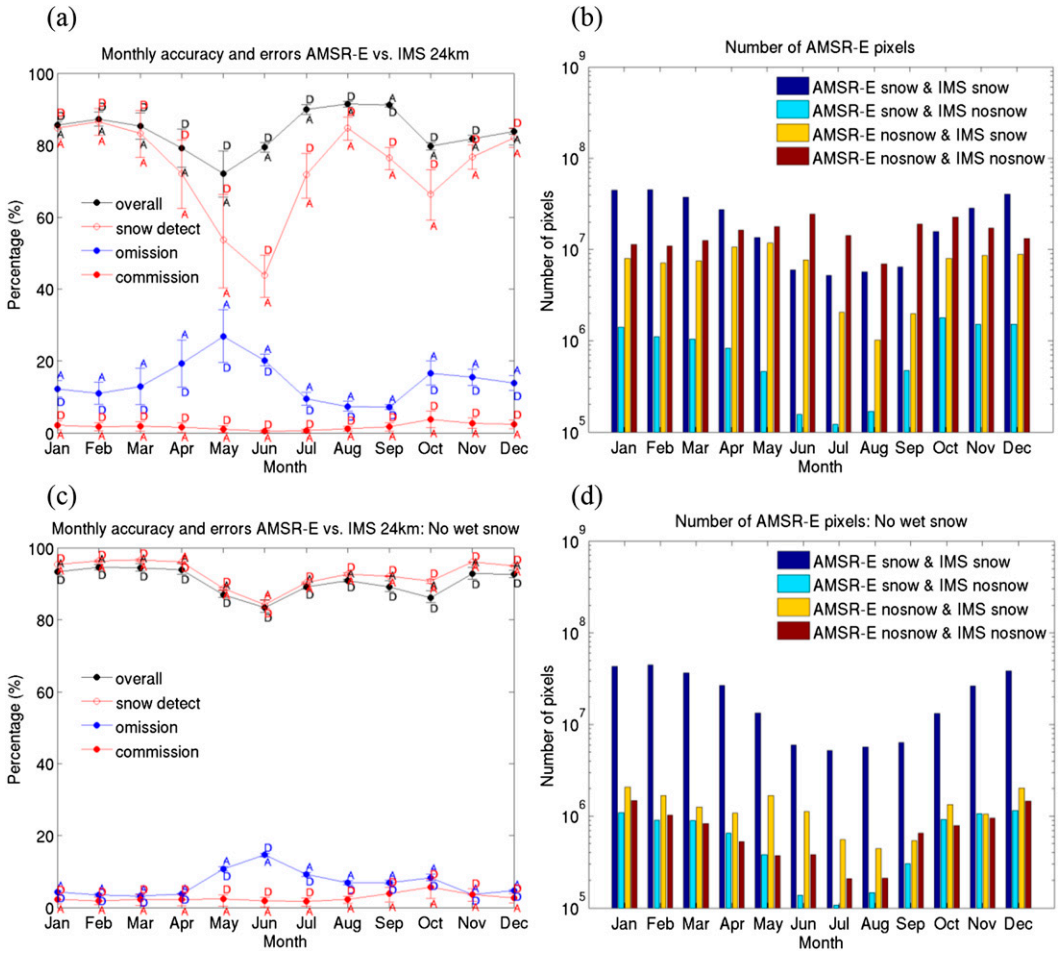

FIG. 3. (a) Monthly comparison between AMSR-E and 24-km IMS SCA: the bars above and below each point indicate descending (''D'') and ascending (''A'') orbits, respectively, and (b) number of AMSR-E pixels. (c),(d) Results when wet snow cases are excluded. Five days (13–17) in each month between June 2002 and September 2011 are included.

(2006) suggested that an atmospheric correction of AMSR-E brightness temperatures is needed for snow cover mapping by considering atmospheric temperature and absorption, and showed that AMSR-E snow cover better matches (7% better) the MODIS product when an atmospheric correction is employed. Savoie et al. (2009) also demonstrated an improvement with an atmospheric correction to SSM/I data. Since the AMSR-E descending orbit is the morning orbit and ascending is the afternoon orbit, the observed difference in SCA accuracy between the two orbits could be due to atmospheric effects on brightness temperatures, which are not accounted for in this version of the algorithm. Therefore, it would be worthwhile to investigate whether the atmospheric correction can explain the difference in SCA accuracy between the two orbits and more importantly if it can improve SCA retrievals.

The incorporation of a snow climatology into the SCA algorithm produces more realistic retrievals. If a snow climatology is not applied, then all pixels over land where snow cannot occur (climatologically) will be included in error statistics calculations, exaggerating the overall accuracy rate and omission error unrealistically. Figure 4 shows the accuracy and error difference between AMSR-E SCA without and with snow climatology using the 24-km IMS data as the reference. The overall accuracy rate of SCA without snow climatology is larger than that of SCA with snow climatology, which is approximately opposite of the omission error difference; meanwhile, the snow detection rate and commission errors are close to zero. Figure 4b shows the increased number of AMSR-E valid pixels over land in error statistics when snow climatology is not applied. The increase in the number of valid AMSR-E pixels (''all cases'') is around 45% in January and 660% in

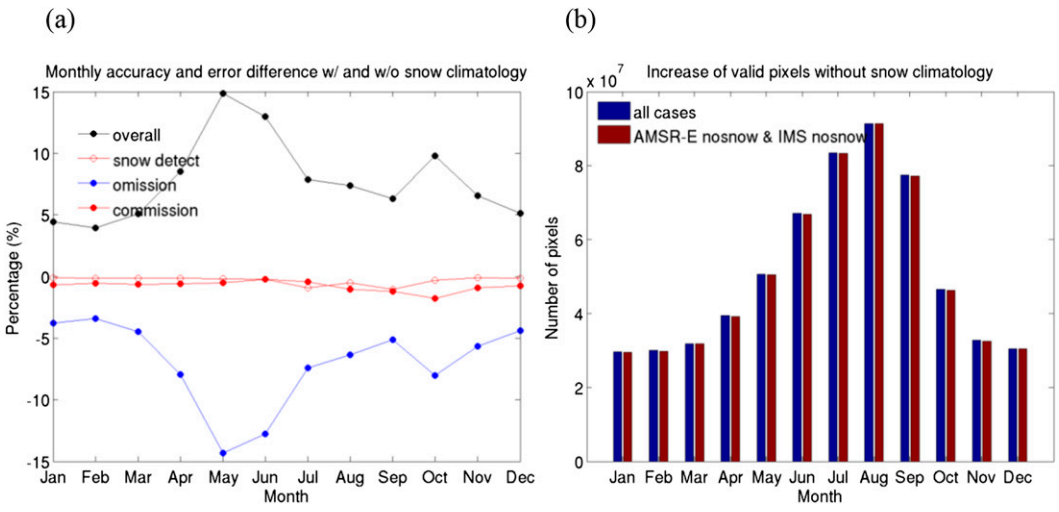

FIG. 4. (a) Monthly accuracy and error difference of SCA with and without snow climatology (without minus with). (b) Increase in the number of valid pixels without snow climatology: blue bars ("all cases") include A, B, C, and D in the confusion table (Table 3) and red bars include only D in the table. Five days (13–17) in each month between June 2002 and September 2011 are included. The 24-km IMS data are used as the reference.

August, mainly because of the inclusion of pixels where both AMSR-E and IMS do not detect snow. The number of valid AMSR-E pixels is 6.51×10^7 in January (1.38×10^7 in August) when snow climatology is applied; meanwhile, the number of valid AMSR-E pixels is increased to 9.47×10^7 in January (1.05×10^8 in August) without snow climatology application. Figure 4b shows the increased number of valid AMSR-E pixels between with and without snow climatology applications, that is, the number difference in valid AMSR-E pixels with and without snow climatology application. The values "45%" and "660%" are calculated by dividing these number differences by the number of valid AMSR-E pixels with snow climatology application. In winter months, the increase in the number of pixels is due to the addition of pixels over land below 20° in latitude, including North Africa, South Asia, the southern part of North America, and the northern part of South America. The (climatologically) snow-impossible area becomes wider poleward during summer months as shown in Fig. 4b. The large difference in overall accuracy rate and omission error shown in Fig. 4a can be explained by the increase in the number of no-snow AMSR-E and IMS pixels. The snow detection rate shows little difference because only the IMS snow pixels are considered. The commission error shows a very slight difference since it is very small with and without snow climatology.

To better understand the error sources, the overall accuracy, snow detection rate, omission error, and commission error for winter months (January, February and December) are shown as a function of elevation (https://lta.cr.usgs.gov/GTOPO30) and forest fraction (Figs. 5 and 6) using 24-km IMS SCA as a reference. Since more than half of AMSR-E snow pixels occur in winter and the general pattern of accuracy and errors during other seasons is similar to winter, statistics are shown only for winter. The overall accuracy and snow detection rate is generally well above 80% up to 3500 m in elevation. The omission error remains between 10% and 20% for all elevation ranges, while the commission error increases sharply above 3500 m. When the wet snow cases are excluded, as expected, the overall accuracy, snow detection rate, and omission error are improved substantially approaching the IMS SCA, and the difference in accuracy between the two orbits decreases (Fig. 5b). On the other hand, the commission error remains similar in magnitude along with a sharp increase above 3500 m.

Wang and Tedesco (2007) showed that passive microwave snow detection is biased at higher elevation (atmospheric effect), and Frei et al. (2012) showed a horizontal distribution of discrepancy between AMSR-E and IMS/MODIS SCA, agreeing with Wang and Tedesco (2007). Savoie et al. (2009) showed that microwave snow cover is overestimated compared to IMS at high elevations. Over AMSR-E-detected dry snow areas, the differences in accuracy/errors between descending and ascending orbits are small in lower elevations and sharply increase above 3500 m. When wet snow cases are included, the descending orbit has a higher overall accuracy, while the ascending orbit shows a higher overall accuracy at lower elevations (<1500 m) than the descending orbit when wet snow

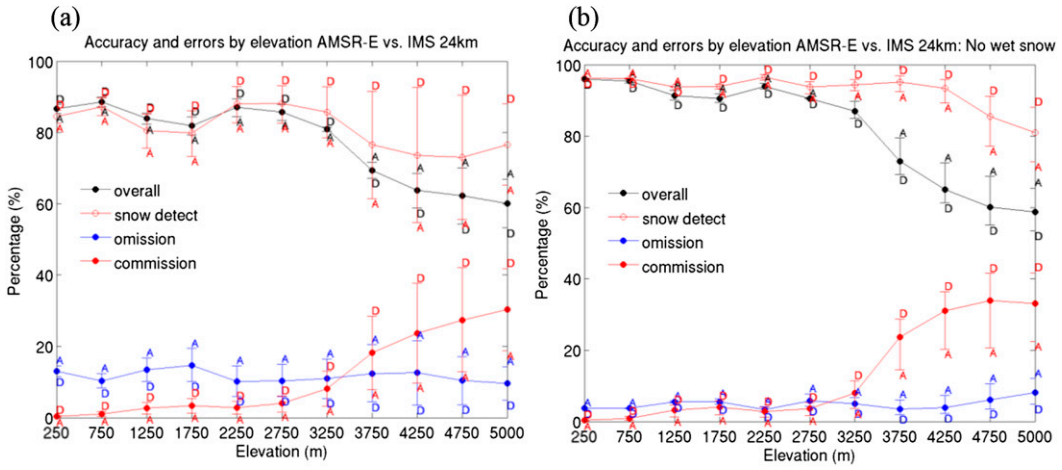

FIG. 5. AMSR-E SCA statistics compared with 24-km IMS product as a function of altitude. Elevation is in 500-m intervals, and the middle value of each interval is shown on the *x* axis; e.g., 250 m indicates an elevation range between 0 and 500 m. The last *x*-axis label, 5000 m, indicates the elevation range over 5000 m. (a) SCA comparison between AMSR-E and IMS: the bars above and below each point indicate descending ("D") and ascending ("A") orbits, respectively. (b) The result after the wet snow criteria is applied. Five days (13–17) in each winter month (January, February, and December) between December 2002 and February 2011 are included.

areas are excluded (Fig. 5b). The wet snow exclusion positively affects the overall accuracy up to 3500 m and also the snow detection rate and omission error in most elevation ranges.

Figure 6 shows AMSR-E SCA statistics as a function of forest fraction. The overall accuracy and snow detection rate are well above 80% for all forest fraction ranges. Omission error slightly increases as the forest fraction increases as shown in Fig. 6a. With the wet snow exclusion, the overall accuracy and snow detection rate are well above 90% and the omission error decreases significantly for all forest fraction ranges (Fig. 6b). The difference in SCA detection between the two orbits also decreases with wet snow exclusion for all forest fraction ranges. The weak dependence of Grody's SCA algorithm performance on forest fraction is an interesting result that could be explained by deeper snow covers associated with

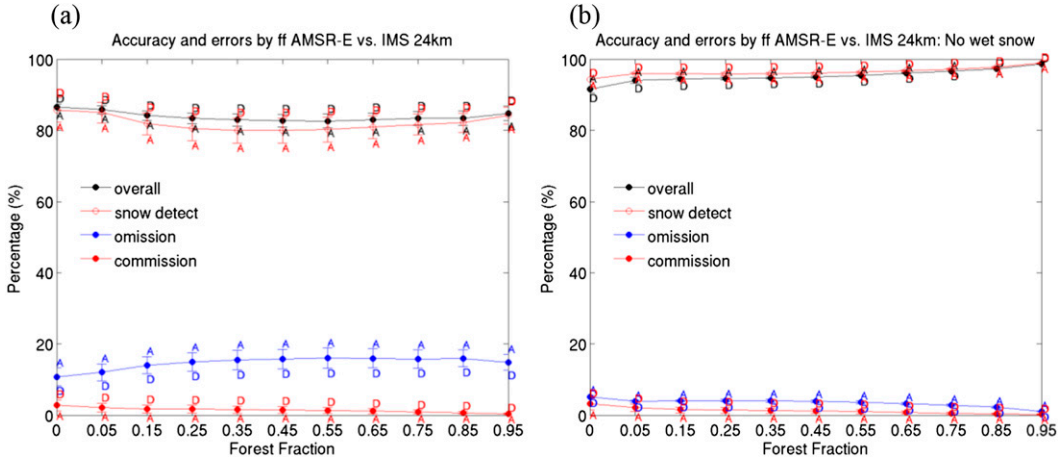

FIG. 6. AMSR-E SCA statistics compared with the 24-km IMS product as a function of forest fraction. Forest fraction is in 0.1 intervals, and the middle value of each interval is shown on the *x* axis; e.g., 0.05 indicates a forest fraction range between 0 and 0.1, except that the leftmost value, 0, on the *x* axis indicates a forest fraction of 0. (a) SCA comparison between AMSR-E and IMS: the bars above and below each point indicate descending ("D") and ascending ("A") orbits, respectively. (b) The result after the wet snow criteria is applied. Five days (13–17) in each winter month (January, February, and December) between December 2002 and February 2011 are included.

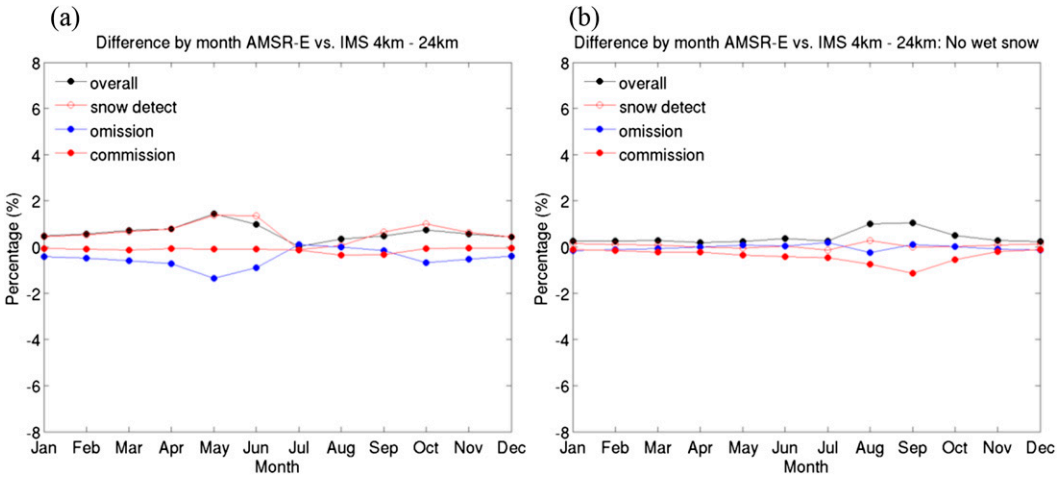

FIG. 7. Monthly accuracy and error difference between AMSR-E vs 24-km IMS and AMSR-E vs 4-km IMS SCA: (a) including wet snow cases and (b) excluding wet snow. A sample of 5 days (13–17) in each month between March 2004 and September 2011 is selected.

more forested terrain and the sensitivity of the 89-GHz channel. Note that Grody's SCA algorithm uses both 37- and 89-GHz channels for mapping snow. Hall et al. (2000) suggested that Grody's SCA algorithm may map the shallower snow cover by the inclusion of the 85-GHz channel of SSM/I instead of using only 37 GHz (Chang et al. 1997; Schweiger and Barry 1989). They also showed that the SSM/I-based Grody SCA algorithm reasonably detects snow cover over forested areas.

Since IMS snow cover data are also available at 4-km horizontal resolution, it is worthwhile to investigate the difference in algorithm performance with respect to 4- and 24-km IMS SCA. The closest IMS pixel to the AMSR-E pixel is selected for comparison between AMSR-E and 4-km IMS SCA. Figure 7 shows the accuracy and error difference between AMSR-E SCA with respect to 4-km IMS and AMSR-E SCA with respect to 24-km IMS. Because the 4-km IMS product is available since March 2004, the period considered in Fig. 7 spans March 2004–September 2011. The number of valid AMSR-E pixels slightly decreases by 0.04% (0.05% for AMSR-E dry snow) with respect to 4-km IMS (not shown). With the inclusion of wet snow cases (Fig. 7a), the overall accuracy, snow detection rate, omission error, and commission error of AMSR-E SCA are slightly improved (mostly within ±1%) with respect to 4-km IMS except in summer months. When wet snow is excluded (Fig. 7b), the difference in accuracy lies within ±0.5%. Even though there are slight improvements in accuracy with respect to 4-km IMS data, the main patterns of the error statistics with respect to 4-km IMS are close to those with respect to 24 km IMS in Fig. 3, indicating that both products could be used as references in large-area assessments of microwave-derived SCA. This result is in agreement with Brown et al.'s (2010) study, which showed less than 10% of monthly difference in SCA between 4- and 24-km IMS data over the Arctic region.

The statistics of AMSR2 SCA (with respect to 24-km IMS) with wet snow exclusion is shown in Fig. 8. AMSR2 SCA also shows significant improvement in the overall accuracy rate, snow detection rate, omission error, and a decreased accuracy difference between descending and ascending orbits with wet snow exclusion, similar to the analysis of AMSR-E SCA. Figures with only the wet snow exclusion are shown. The overall accuracy rate of monthly AMSR2 SCA is well above 80% every month and over 90% in winter months (Fig. 8a). AMSR2 SCA shows the overall accuracy rate above 80% up to 3500 m (Fig. 8b) and above 90% for all forest fraction ranges (Fig. 8c) in winter months.

A regional assessment of AMSR-E SCA is performed for various snow cover classes. Sturm et al. (1995) classify snow cover into six classes: tundra, taiga, Alpine, prairie, maritime, and ephemeral. Each snow class possesses distinct physical properties—depth, density, and stratigraphy—that in combination should impact the ability of microwave measurements for mapping snow differently. Note that Grody's SCA algorithm as well as other operational passive microwave algorithms does not account for these snowpack properties that are known to influence passive microwave measurements. The Sturm et al. (1995) snow classification

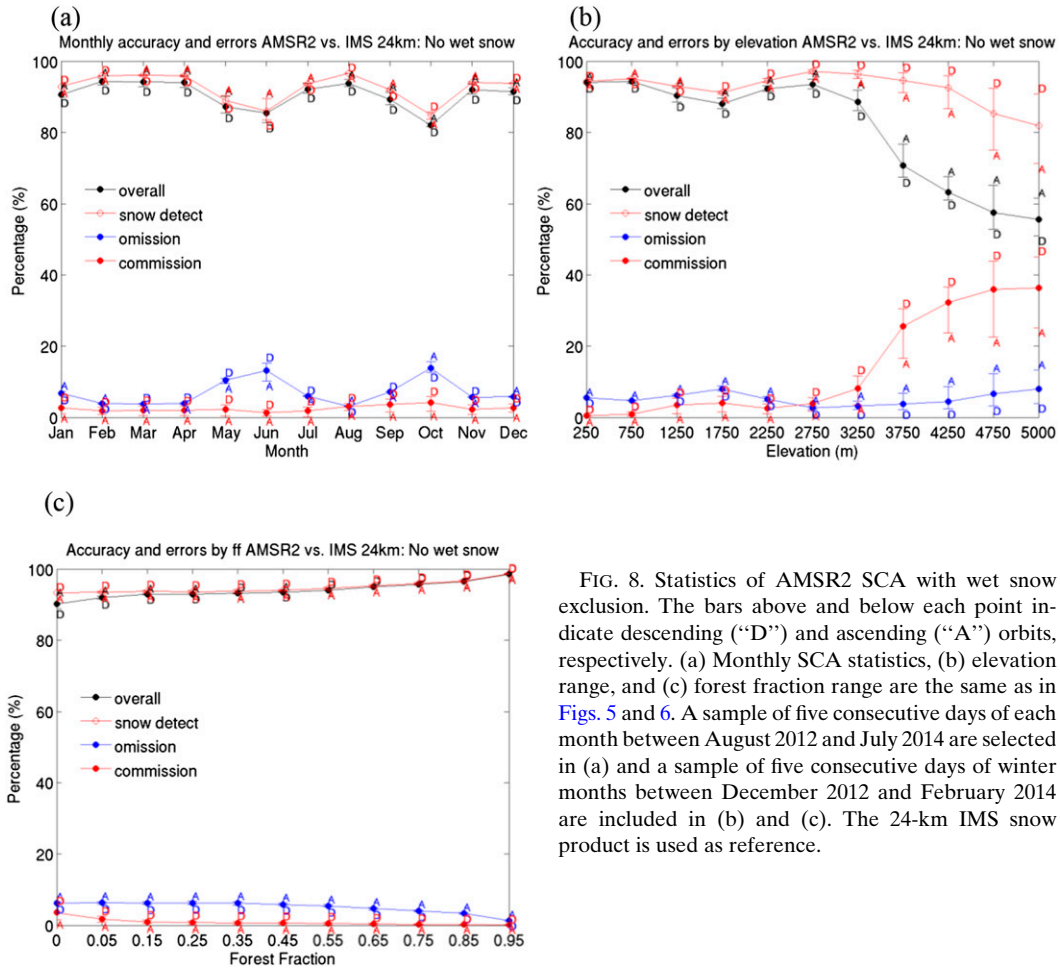

FIG. 8. Statistics of AMSR2 SCA with wet snow exclusion. The bars above and below each point indicate descending ("D") and ascending ("A") orbits, respectively. (a) Monthly SCA statistics, (b) elevation range, and (c) forest fraction range are the same as in Figs. 5 and 6. A sample of five consecutive days of each month between August 2012 and July 2014 are selected in (a) and a sample of five consecutive days of winter months between December 2012 and February 2014 are included in (b) and (c). The 24-km IMS snow product is used as reference.

map at 0.5° resolution was obtained from the National Snow and Ice Data Center (NSIDC) and was used to compute error statistics with respect to 24-km IMS SCA.

Table 4 summarizes error statistics and mean surface temperature for each snow cover class. The error statistics exclude wet snow cases. Surface air temperature is estimated by applying AMSR-E microwave brightness temperatures to a simple linear regression algorithm (Kelly 2009). In Table 4, labels A, B, C and D denote detection rate categories (same as those in Table 3) when both AMSR-E and IMS detect snow, AMSR-E detects snow and IMS detects no snow, AMSR-E detects no snow and IMS detects snow, and both AMSR-E and IMS detect no snow, respectively. The highest overall accuracy is shown for taiga snow class (97.4%) followed by tundra (96.4%) and the lowest accuracy for ephemeral (71.7%). The statistics for category A (correct snow detection rate) are negatively associated with mean surface temperature: taiga has the lowest mean surface temperature and ephemeral the highest. This surface temperature dependence could be explained by a higher rate of snow misses in a warmer weather snow cover (more frequent wet snow cases) and/or by the indirect effect of surface temperature on snow properties that impact passive microwave measurements, for example, snow metamorphism. For example, taiga and tundra snow covers are associated with a larger snow grain size parameter than other snow cover classes (Sturm et al. 1995), which produces a stronger microwave scattering signal and a higher snow detection rate (Josberger et al. 1996).

b. *Assessment of SD*

Figures 9–11 present AMSR-E SD performance statistics (RMS error and bias) for SD less than 100 cm with respect to elevation, forest fraction, and the magnitude of in situ SD over AMSR-E-detected dry snow, respectively. Since more than 75% of the total number of AMSR-E pixels with valid SD occurs during winter months, the results are shown for only winter months. Overall, the RMS error is 19.90 cm and the bias is

TABLE 4. Mean surface air temperature for each snow cover classification. A, B, C, D are indices corresponding to the confusion matrices in Table 3. Mean surface air temperatures are calculated based on AMSR-E measurements (Kelly 2009) for the period between June 2002 and September 2011. The value in parenthesis shows the percentage of the number of each category divided by the total number of pixels. The overall accuracy rate is the sum of the percentage values in A and D.

	Temp for A (K)	Temp for B (K)	Temp for C (K)	Temp for D (K)	Overall accuracy (%)
Tundra	249.2 (93.0%)	259.6 (1.2%)	263.5 (4.2%)	270.1 (1.6%)	94.6%
Taiga	247.4 (96.7%)	258.1 (0.9%)	264.6 (1.7%)	273.4 (0.7%)	97.4%
Maritime	255.4 (78.4%)	258.9 (4.0%)	262.0 (15.1%)	268.8 (2.5%)	80.9%
Ephemeral	253.1 (40.3%)	256.8 (22.2%)	264.6 (6.1%)	270.3 (31.4%)	71.7%
Prairie	254.5 (56.1%)	256.6 (14.3%)	262.6 (11.7%)	265.7 (17.9%)	74.0%
Alpine	256.9 (85.2%)	258.1 (3.8%)	265.5 (9.3%)	267.8 (1.7%)	86.9%

1.16 cm. Statistics for the descending and ascending orbits are similar: the RMS errors are 19.93 and 19.86 cm, and the biases are 1.81 and 0.26 cm for the descending and ascending orbits, respectively.

It is important to note that 70% of AMSR-E pixels collocated to in situ SD are located in the low-elevation range between 0 and 500 m, which substantially influences the overall statistics (Fig. 9b). This lower-elevation bias is a general concern arising from the distribution of in situ SD–measuring stations skewed toward lower elevations. AMSR-E SD is overestimated for elevations between 500 and 2500 m and underestimated for elevations above 2500 m. The negative bias and RMS error increase with elevation above 1500 m (Fig. 9a). Figures 9c and 9d show histograms of in situ SD for elevation ranging between 500 and 1000 m and 2500 and 3000 m, respectively. The large number of in situ SD values less than 10 cm located between 500 and 1000 m could explain the positive SD bias in this elevation range. On the other hand, the distribution of in situ SD between 2500 and 3000 m (a larger portion of in situ stations have a larger SD) could explain the negative SD bias.

The effect of forest fraction on AMSR-E SD is shown in Fig. 10. As forest fraction increases, RMS error increases and bias decreases below zero, which indicates that the masking effect of the forest canopy on passive microwave brightness temperature can be a source of error for SD estimation (Foster et al. 2005; Kelly 2009; Tedesco and Narvekar 2010). AMSR-E SD is overestimated over low forest fraction (below 0.4) pixels and underestimated for forest fraction above 0.5, with the magnitude of underestimation increasing as forest fraction increases. The positive bias over low forest fraction pixels could also be explained by the SD magnitude effect—the predominance of small in situ SD values over low forest fraction pixels in our sample and the overestimation of shallow snow covers by Kelly's SD algorithm (Fig. 10c). Derksen (2008) showed that the brightness temperature difference between 36.5 and 18.7 GHz is reduced with denser forest fraction. Note that this brightness temperature difference is used to compute forest SD in Eq. (1) and thus the underestimation of AMSR-E SD is closely related to the forest fraction term as the forest fraction increases. Derksen (2008) also showed that the brightness temperature pair of AMSR-E 18.7 and 10.7 GHz can be used over the boreal forest area; therefore, it would be worthwhile to consider these channels in the forest fraction term in Eq. (1).

In Fig. 11, SD statistics are shown as a function of in situ SD. RMS error and bias increase in magnitude as SD increases, especially for large in situ SD, and this dependence is much stronger than the dependence of RMS error and bias on forest fraction and elevation. It also shows that reliable SD estimation for snow deeper than 50 cm remains a challenge despite the use of lower AMSR-E frequencies (10.7 and 18.7 GHz) over the nonforested snow component in Eq. (1). The magnitude of RMS error is generally larger than half of the middle SD value of each in situ SD range. Kelly et al. (2003) showed similar results of RMS error dependence on the magnitude of SD and suggested two possible reasons: microwave saturation at SD greater than 50–100 cm (depending on grain size and density) and the spatial limitation of in situ SD data to be representative of the AMSR-E pixel resolution. Both descending and ascending orbits are generally close in bias and RMS error; for example, the difference of both bias and RMS error are less than 1 cm in magnitude except for the large SD range (>90 cm).

The performance statistics for AMSR2 SD are shown for dry snow cases as a function of elevation, forest fraction, and in situ SD for winter months in Figs. 12a–c, respectively. The pattern of variation of AMSR2 SD bias and RMS error with respect to each factor is similar to that of AMSR-E (Figs. 9a–11a) except for some differences in magnitude. For example, AMSR2 SD shows bias values over 10 cm at elevation ranges between 500 and 2000 m (Fig. 12a), whereas AMSR-E SD bias is smaller than 10 cm for this elevation range (Fig. 9a). Above

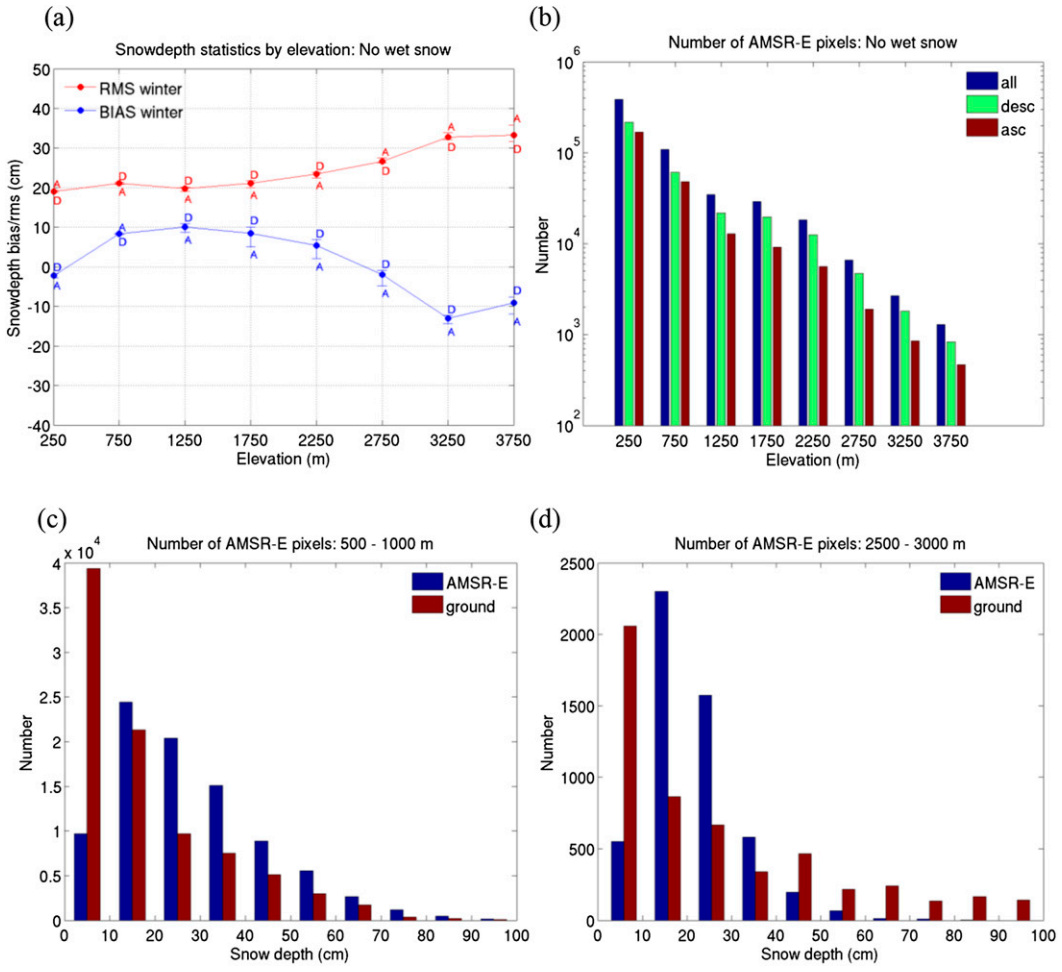

FIG. 9. (a) Snow depth statistics by elevation: the bars above and below each point indicate descending (''D'') and ascending (''A'') orbits, respectively. (b) The number of AMSR-E pixels corresponding to the ground truth observations. SYNOP stations and U.S. COOP stations are considered as the ground truth. Elevation in 500-m intervals, and the middle value of each interval is shown on the *x* axis; e.g., 250 m indicates an elevation range between 0 and 500 m. Snow depth histogram is shown for elevation range (c) between 500 and 1000 m and (d) between 2500 and 3000 m. A sample of five consecutive days (13–17) in each winter month (January, February, and December) between December 2002 and February 2011 is selected.

2500 m, RMS error of AMSR2 SD is smaller than that of AMSR-E SD. AMSR2 SD RMS error slightly decreases for forest fraction above 0.4 (Fig. 12b), whereas AMSR-E SD RMS error slightly increases (Fig. 10a). With respect to in situ SD, the pattern of variation in RMS and bias is strikingly similar (Figs. 12c and 11a), both indicating a strong dependence of these performance measures on the magnitude of SD for snow deeper than 50 cm.

Table 5 shows AMSR-E SD performance statistics for each snow cover class. Positive (negative) bias means that AMSR-E retrieval overestimates (underestimates) SD. Each snow cover class has RMS error values between 18 and 22 cm except ephemeral snow (15 cm). Ephemeral snow areas have smaller SD compared to other snow classes and a smaller number of valid AMSR-E pixels. On the other hand, biases differ among the snow classes in both magnitude and direction. Ephemeral, tundra, taiga, and prairie snow classes have a positive bias, whereas Alpine and maritime snow classes have a negative bias. The ephemeral snow class has the largest positive bias and the maritime snow class the largest negative bias. Dong et al. (2005) also showed that maritime has the largest (negative) mean error of microwave SWE among snow classes since the maritime area is in warmer climates near open water bodies. These results demonstrate that the dynamic parameterizations for $p1$ and $p2$ coefficients in Eq. (2) may not be sufficiently robust and may need

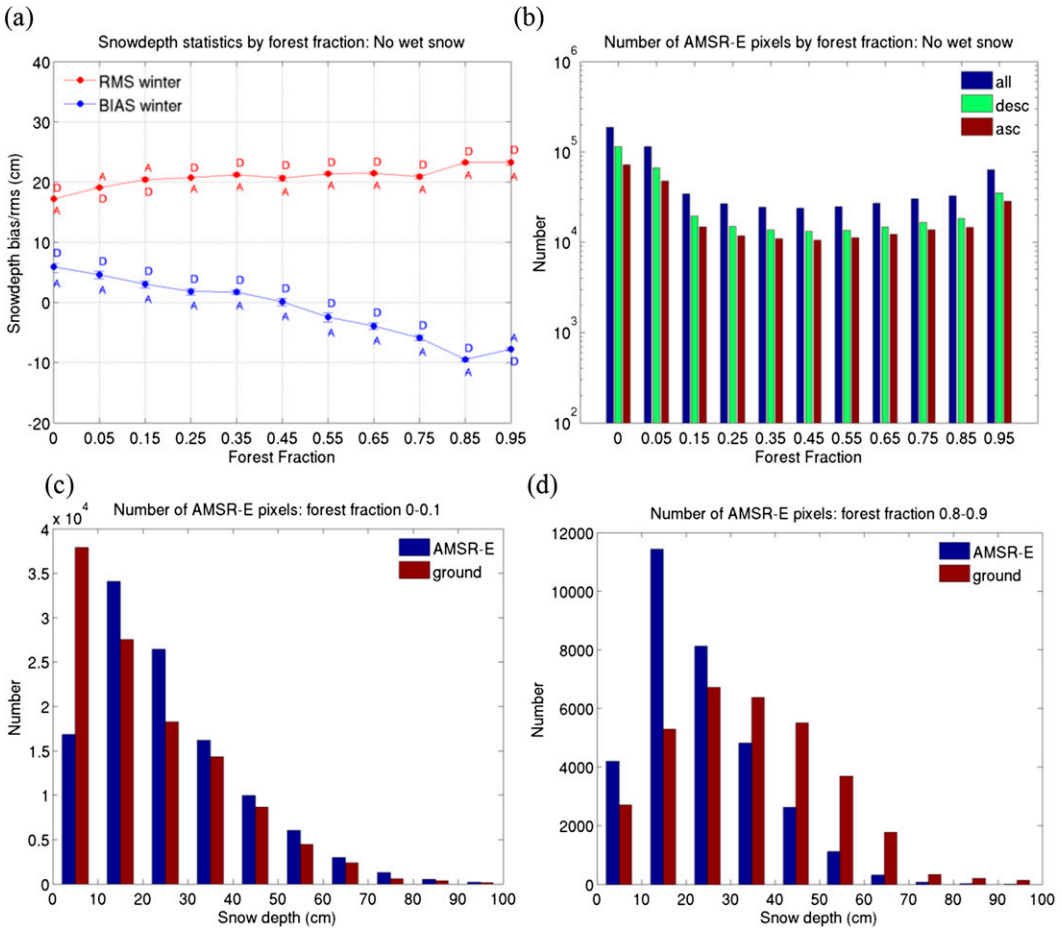

FIG. 10. (a) Snow depth statistics by forest fraction: the bars above and below each point indicate descending ("D") and ascending ("A") orbits, respectively. (b) The number of AMSR-E pixels corresponding to the ground truth observations. Ground site SD are considered as the ground truth. Forest fraction in 0.1 intervals, and the middle value of each interval is shown on the *x* axis; e.g., 0.05 indicates a forest fraction range between 0 and 0.1, except that the leftmost value, 0, on the *x* axis indicates a forest fraction of 0. Snow depth histogram is shown for forest fraction range (c) between 0 and 0.1 and (d) between 0.8 and 0.9. A sample of five consecutive days (13–17) in each winter month (January, February, and December) between December 2002 and February 2011 is selected.

readjustment. For example, they could be adjusted seasonally and regionally for each snow class. Additionally, the use of AMSR-E/AMSR2 lower-frequency channels in the forest element should also be tested.

4. Summary and conclusions

This study presents an in-depth assessment of AMSR2 algorithms for the retrieval of snow-covered area (SCA) and snow depth (SD) that will be used operationally by the National Oceanic and Atmospheric Administration (NOAA). AMSR2 on board the *Global Change Observation Mission 1st–Water* or "*Shizuku*" (*GCOM-W1*) satellite is a follow-on instrument to NASA's AMSR-E with a similar channel configuration, improved calibration system, and improved spatial resolution. The SCA algorithm is based on NOAA's heritage microwave algorithm with snow climatology tests and wet snow filtering as new enhancements. The SD algorithm is adopted from the current version of the NASA AMSR-E operational SWE algorithm.

Quantitative assessment of the algorithms was performed for a 10-yr period for AMSR-E and a 2-yr period for AMSR2 using the NOAA's Interactive Multisensor Snow and Ice Mapping System (IMS) 24- and 4-km snow cover products and in situ SD data as "ground truth" references. Evaluation results for AMSR-E SCA with respect to IMS showed the overall accuracy rate to be generally above 80%. The overall accuracy rate and snow detection rate are much closer to the IMS (above

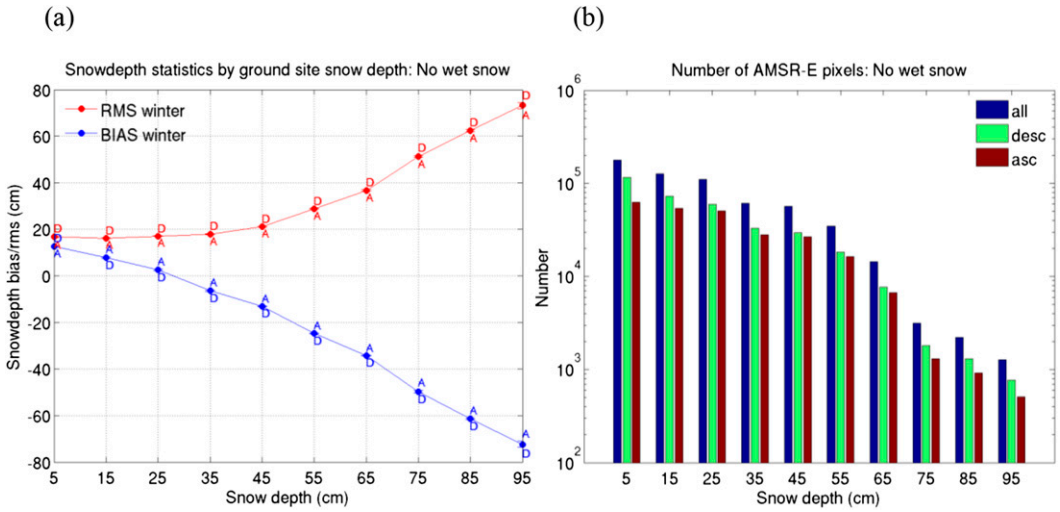

FIG. 11. (a) Snow depth statistics by in situ SD: the bars above and below each point indicate descending (''D'') and ascending (''A'') orbits, respectively. (b) The number of AMSR-E pixels corresponding to the ground truth observations. In situ SD is divided into 10-cm intervals, and the middle value of each interval is shown on the *x* axis; e.g., 15 indicates an elevation range between 10 and 20 cm. A sample of five consecutive days (13–17) in each winter month (January, February, and December) between December 2002 and February 2011 is selected.

90% in winter months) when wet snow cases are excluded. In addition, the difference in SCA accuracy between the descending and ascending orbits decreases significantly when wet snow areas are excluded, though the descending orbit still shows a smaller omission error and larger commission error than the ascending orbit. The omission error exhibits a seasonal pattern where it decreases as winter progresses, while the commission error is nearly constant (around 5%). Performance statistics show no dependency on elevation up to 3500 m, with an omission error between 10% and 20% and a commission error around 5%. Above 3500 m, the commission error increases sharply. Performance statistics also show only a weak dependence on forest fraction. This apparent contradiction to other studies could be attributed in part to a higher sensitivity of the 89-GHz channel to snow cover than the 37 GHz used by other algorithms.

With respect to snow classes, the highest overall accuracy rate was shown for the taiga snow class, followed by tundra; the lowest accuracy rate was for the ephemeral snow class. The correct snow detection rate was negatively associated with mean surface temperature: taiga had the lowest mean surface temperature and ephemeral the highest. This surface temperature dependence could be explained by a higher rate of snow misses in a warmer weather snow cover (more frequent wet snow cases) and/or by the indirect effect of surface temperature on snow properties that impact passive microwave measurements, for example, snow metamorphism. Incorporation of a snow climatology into the SCA algorithm is recommended because it produces more realistic results. AMSR-E SD error statistics (RMS error and bias) with respect to in situ measured SD show a dependence on elevation, forest fraction, in situ SD, and snow cover class. RMS error increases with elevation, forest fraction and the magnitude of in situ SD. Bias dependence on elevation and forest fraction were explained by the SD distribution. Positive bias for low-elevation and low forest fraction areas was attributed to the predominance of shallow snow covers and the negative bias over high-elevation and high forest fraction areas was attributed to the predominance of deeper snow covers. The positive bias over ephemeral snow and the negative bias over maritime snow covers could also be partially attributed to reduced sensitivity to shallow and deep snow, respectively. Saturation of the microwave SD signal to deeper snow remains a fundamental unresolved problem despite the use of AMSR-E low-frequency microwave channels. The AMSR2 SCA and SD comparisons to in situ SD show similar results to those of AMSR-E, although the dependence of error statistics on elevation and forest fraction are somewhat different. Given the climatic controls on the regional distribution of snow cover, a reasonable strategy to improve the retrieval accuracy of SD and SCA would be regional adjustment of Grody's SCA and Kelly's SD algorithm coefficients for use with AMSR2.

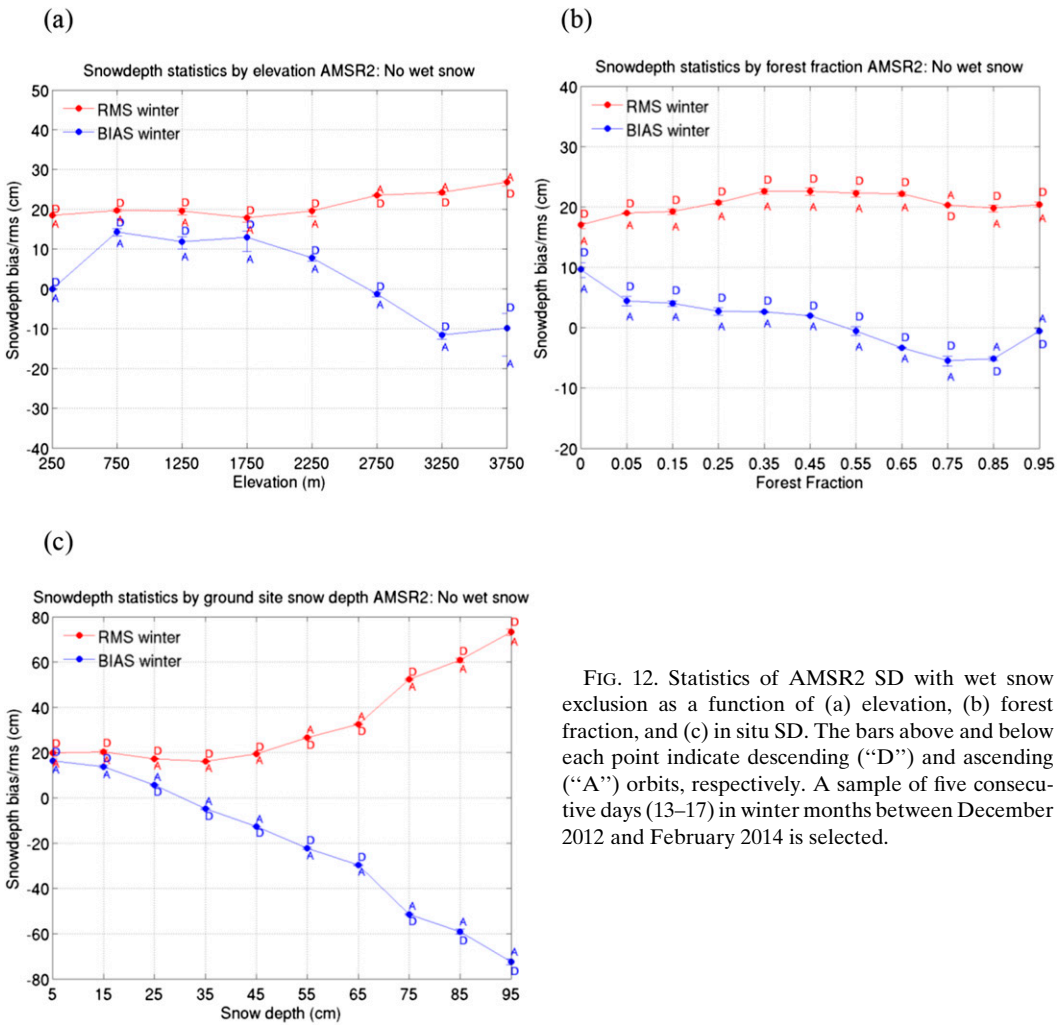

FIG. 12. Statistics of AMSR2 SD with wet snow exclusion as a function of (a) elevation, (b) forest fraction, and (c) in situ SD. The bars above and below each point indicate descending ("D") and ascending ("A") orbits, respectively. A sample of five consecutive days (13–17) in winter months between December 2012 and February 2014 is selected.

Several other factors need further investigation. The utility of applying an atmospheric correction to the SCA algorithm (and perhaps to the SD algorithm as well) needs to be evaluated. Regional and perhaps seasonal adjustment of dynamic algorithm coefficients for 18.7- and 10.7-GHz brightness temperatures may improve estimated SD, especially for deeper snow.

Acknowledgments. This work was funded under the National Oceanic and Atmospheric Administration Cooperative Agreement NA10NES4400013 by the Joint Polar Satellite System (JPSS) program. The views, opinions, and findings contained in this report are those of the author(s) and should not be construed as an official National Oceanic and Atmospheric Administration or U.S. government position, policy, or decision.

TABLE 5. Mean bias and RMS error of SD comparison between AMSR-E measured and in situ observed (AMSR-E minus in situ observation) for each snow cover classification. Statistical values are based on AMSR-E measurements for the winter months (December, January, and February) between December 2002 and February 2011.

	RMSE (cm)	Bias (cm)	Mean (cm) in situ observation	No. of valid AMSR-E pixels
Tundra	18.77	4.51	25.10	96 282
Taiga	20.96	3.77	29.18	16 4758
Maritime	19.37	−5.34	20.20	99 887
Ephemeral	14.95	6.05	8.40	3876
Prairie	18.93	2.75	18.49	15 8219
Alpine	21.97	−4.45	25.14	64 195

REFERENCES

Armstrong, R. L., and M. J. Brodzik, 2001: Recent northern hemisphere snow extent: A comparison of data derived from visible and microwave satellite sensors. *Geophys. Res. Lett.*, **28**, 3673–3676, doi:10.1029/2000GL012556.

Barry, R. G., 2002: The role of snow and ice in the global climate system: A review. *Polar Geogr.*, **26**, 235–246, doi:10.1080/789610195.

——, R. Armstrong, T. Callaghan, J. Cherry, S. Gearhead, A. Nolin, D. Russell, and C. Zockler, 2007: Snow. Global outlook for ice and snow, United Nations Environment Programme Publ., 39–62.

Brasnett, B., 1999: A global analysis of snow depth for numerical weather prediction. *J. Appl. Meteor.*, **38**, 726–740, doi:10.1175/1520-0450(1999)038<0726:AGAOSD>2.0.CO;2.

Brown, R., C. Derksen, and L. Wang, 2010: A multi-data set analysis of variability and change in Arctic spring snow cover extent, 1967-2008. *J. Geophys. Res.*, **115**, D16111, doi:10.1029/2010JD013975.

Chang, A. T. C., J. L. Foster, and D. K. Hall, 1987: Nimbus-7 SMMR derived global snow cover parameters. *Ann. Glaciol.*, **9**, 39–44.

——, ——, ——, B. E. Goodison, A. E. Walker, and J. R. Metcalfe, 1997: Snow parameters derived from microwave measurements during the BOREAS winter field experiment. *J. Geophys. Res.*, **102**, 29 663–29 671, doi:10.1029/96JD03327.

Cohen, J., 1994: Snow cover and climate. *Weather*, **49**, 150–156, doi:10.1002/j.1477-8696.1994.tb05997.x.

——, and D. Entekhabi, 1999: Eurasian snow cover variability and Northern Hemisphere climate predictability. *Geophys. Res. Lett.*, **26**, 345–348, doi:10.1029/1998GL900321.

Derksen, C., 2008: The contribution of AMSR-E 18.7 and 10.7 GHz measurements to improved boreal forest snow water equivalent retrievals. *Remote Sens. Environ.*, **112**, 2701–2710, doi:10.1016/j.rse.2008.01.001.

——, E. LeDrew, A. Walker, and B. Goodison, 2000: Influence of sensor overpass time on passive microwave-derived snow cover parameters. *Remote Sens. Environ.*, **71**, 297–308, doi:10.1016/S0034-4257(99)00084-X.

Dong, J., J. P. Walker, and P. R. Houser, 2005: Factors affecting remotely sensed snow water equivalent uncertainty. *Remote Sens. Environ.*, **97**, 68–82, doi:10.1016/j.rse.2005.04.010.

Dyer, J., 2008: Snow depth and streamflow relationships in large North American watersheds. *J. Geophys. Res.*, **113**, D18113, doi:10.1029/2008JD010031.

Ferraro, R. R., and Coauthors, 2005: NOAA operational hydrological products derived from the AMSU. *IEEE Trans. Geosci. Remote Sens.*, **43**, 1036–1049, doi:10.1109/TGRS.2004.843249.

Foster, J. L., D. K. Hall, and A. T. C. Chang, 1984: An overview of passive microwave snow research and results. *Rev. Geophys. Space Phys.*, **22**, 195–208, doi:10.1029/RG022i002p00195.

——, C. Sun, J. P. Walker, R. Kelly, A. Chang, J. Dong, and H. Powell, 2005: Quantifying the uncertainty in passive microwave snow water equivalent observations. *Remote Sens. Environ.*, **94**, 187–203, doi:10.1016/j.rse.2004.09.012.

Frei, A., M. Tedesco, S. Lee, J. Foster, D. K. Hall, R. Kelly, and D. A. Robinson, 2012: A review of global satellite-derived snow products. *Adv. Space Res.*, **50**, 1007–1029, doi:10.1016/j.asr.2011.12.021.

Grody, N. C., 1991: Classification of snow cover and precipitation using the Special Sensor Microwave Imager. *J. Geophys. Res.*, **96**, 7423–7435, doi:10.1029/91JD00045.

——, and A. N. Basist, 1996: Global identification of snowcover using SSM/I measurements. *IEEE Trans. Geosci. Remote Sens.*, **34**, 237–249, doi:10.1109/36.481908.

——, F. Weng, and R. Ferraro, 2000: Application of AMSU for obtaining hydrological parameters. *Microwave Radiometry and Remote Sensing of the Earth's Surface and Atmosphere*, P. Pampaloni and S. Paloscia, Eds., VSP, 339 –351.

Hall, D. K., A. B. Tait, J. L. Foster, A. T. C. Chang, and M. Allen, 2000: Intercomparison of satellite-derived snow-cover maps. *Ann. Glaciol.*, **31**, 369–376, doi:10.3189/172756400781820066.

Hamlet, A. F., and D. P. Lettenmaier, 1999: Effects of climate change on hydrology and water resources in the Columbia River basin. *J. Amer. Water Resour. Assoc.*, **35**, 1597–1623, doi:10.1111/j.1752-1688.1999.tb04240.x.

Helfrich, S. R., D. McNamara, B. H. Ramsay, T. Baldwin, and T. Kasheta, 2007: Enhancements to, and forthcoming developments in the Interactive Multisensor Snow and Ice Mapping System (IMS). *Hydrol. Processes*, **21**, 1576–1586, doi:10.1002/hyp.6720.

Hollinger, J. P., J. L. Peirce, and G. A. Poe, 1990: SSM/I instrument evaluation. *IEEE Trans. Geosci. Remote Sens.*, **28**, 781–790, doi:10.1109/36.58964.

Imaoka, K., M. Kachi, M. Kasahara, N. Ito, K. Nakagawa, and T. Oki, 2010: Instrument performance and calibration of AMSR-E and AMSR2. *ISPRS Technical Commission VIII Symposium: Networking the World with Remote Sensing*, K. Kajiware et al., Eds., Vol. XXXVIII, Part 8, ISPRS, 13–16.

IPCC, 2007: *Climate Change 2007: The Physical Science Basis*. Cambridge University Press, 996 pp.

Josberger, E. G., P. Gloersen, A. Chang, and A. Rango, 1996: The effects of snowpack grain size on satellite passive microwave observations from the Upper Colorado River Basin. *J. Geophys. Res.*, **101**, 6679–6688, doi:10.1029/95JC02959.

Kelly, R. E., 2009: The AMSR-E snow depth algorithm description and initial results. *J. Remote Sens. Soc. Japan*, **29**, 307–317, doi:10.11440/rssj.29.307.

——, A. T. Chang, L. Tsang, and J. L. Foster, 2003: A prototype AMSR-E global snow area and snow depth algorithm. *IEEE Trans. Geosci. Remote Sens.*, **41**, 230–242, doi:10.1109/TGRS.2003.809118.

Kongoli, C., and S. Helfrich, 2015: A multi-source interactive analysis approach for Northern Hemispheric snow depth estimation. *Proc. IGARSS 2015: Remote Sensing; Understanding the Earth for a Safer World*, Milan Italy, IGARSS, MOP.PO.10. [Available online at http://www.igarss2015.org/Papers/viewpapers.asp?papernum=8441.]

——, C. A. Dean, S. R. Helfrich, and R. R. Ferraro, 2007: Evaluating the potential of a blended passive microwave-interactive multi-sensor product for improved mapping of snow cover and estimations of snow water equivalent. *Hydrol. Processes*, **21**, 1597–1607, doi:10.1002/hyp.6722.

——, P. Romanov, and R. Ferraro, 2012: Snow cover monitoring from remote-sensing satellites. *Remote Sensing and Drought: Innovative Monitoring Approaches*, B. Wardlow, M. Anderson, and J. Verdin, Eds., CRC Press, 359–386.

LCSCG, 2012: User guide for the MODIS Land Cover Type Product (MCD12Q1). Land Cover and Surface Climate Group, Boston University. [Available online at http://www.bu.edu/lcsc/files/2012/08/MCD12Q1_user_guide.pdf.]

Liang, T., X. Zhang, H. Xie, C. Wu, Q. Feng, X. Huang, and Q. Chen, 2008: Toward improved daily snow cover mapping with advanced combination of MODIS and AMSR-E

measurements. *Remote Sens. Environ.*, **112**, 3750–3761, doi:10.1016/j.rse.2008.05.010.

Markus, T., D. C. Powell, and J. R. Wang, 2006: Sensitivity of passive microwave snow depth retrievals to weather effects and snow evolution. *IEEE Trans. Geosci. Remote Sens.*, **44**, 68–77, doi:10.1109/TGRS.2005.860208.

NOHRSC, 2004: Snow Data Assimilation System (SNODAS) data products at NSIDC. National Snow and Ice Data Center, Boulder, CO, digital media, doi:10.7265/N5TB14TC.

Ramsay, B., 1998: The interactive multisensor snow and ice mapping system. *Hydrol. Processes*, **12**, 1537–1546, doi:10.1002/(SICI)1099-1085(199808/09)12:10/11<1537::AID-HYP679>3.0.CO;2-A.

Savoie, M. H., R. L. Armstrong, M. J. Brodzik, and J. R. Wang, 2009: Atmospheric corrections for improved satellite passive microwave snow cover retrievals over the Tibet Plateau. *Remote Sens. Environ.*, **113**, 2661–2669, doi:10.1016/j.rse.2009.08.006.

Schweiger, A. J., and R. G. Barry, 1989: Evaluation of algorithms for mapping snow cover parameters in the Federal Republic of Germany using passive microwave data. *Erdkunde*, **43**, 85–94, doi:10.3112/erdkunde.1989.02.02.

Sturm, M., J. Holmgren, and G. E. Liston, 1995: A seasonal snow cover classification system for local to global applications. *J. Climate*, **8**, 1261–1283, doi:10.1175/1520-0442(1995)008<1261:ASSCCS>2.0.CO;2.

Sun, N., and F. Weng, 2008: Evaluation of Special Sensor Microwave Imager/Sounder (SSMIS) environmental data records. *IEEE Trans. Geosci. Remote Sens.*, **46**, 1006–1016, doi:10.1109/TGRS.2008.916984.

Tedesco, M., and J. R. Wang, 2006: Atmospheric correction of AMSR-E brightness temperatures for dry snow cover mapping. *IEEE Geosci. Remote Sens. Lett.*, **3**, 320–324, doi:10.1109/TGRS.2008.917368.

——, and P. S. Narvekar, 2010: Assessment of the NASA AMSR-E SWE product. *IEEE J. Sel. Top. Appl. Earth Obs. Remote Sens.*, **3**, 141–159, doi:10.1109/JSTARS.2010.2040462.

Townshend, J., M. Hansen, M. Carroll, C. DiMiceli, R. Sohlberg, and C. Huang, 2011: User guide for the MODIS Vegetation Continuous Fields product: Collection 5 version 1. University of Maryland. [Available online at http://glcf.umd.edu/library/guide/VCF_C5_UserGuide_Dec2011.pdf.]

Vuyovich, C. M., and J. M. Jacobs, 2011: Snowpack and runoff generation using AMSR-E passive microwave observations in the Upper Helmand Watershed, Afghanistan. *Remote Sens. Environ.*, **115**, 3313–3321, doi:10.1016/j.rse.2011.07.014.

——, ——, and S. F. Daly, 2014: Comparison of passive microwave and modeled estimates of total watershed SWE in the continental United States. *Water Resour. Res.*, **50**, 9088–9102, doi:10.1002/2013WR014734.

Walsh, J. E., 1984: Snow cover and atmospheric variability: Changes in the snow covering the earth's surface affect both daily weather and long-term climate. *Amer. Sci.*, **72**, 50–57.

Wang, J. R., and M. Tedesco, 2007: Identification of atmospheric influences on the estimation of snow water equivalent from AMSR-E measurements. *Remote Sens. Environ.*, **111**, 398–408, doi:10.1016/j.rse.2006.10.024.

Yang, D., D. Robinson, Y. Zhao, T. Estilow, and B. Ye, 2003: Streamflow response to seasonal snow cover extent change in large Siberian watersheds. *J. Geophys. Res.*, **108**, 4578, doi:10.1029/2002JD003149.

Zhang, X., K. D. Harvey, W. D. Hogg, and T. R. Yuzyk, 2001: Trends in Canadian streamflow. *Water Resour. Res.*, **37**, 987–998, doi:10.1029/2000WR900357.